Conformal Coating on Ultrahigh-Aspect-Ratio Nanopores of Anodic Alumina by Atomic Layer Deposition

J. W. Elam,[†] D. Routkevitch,[§] P. P. Mardilovich,[§,||] and S. M. George*[,†,‡]

Department of Chemistry and Biochemistry and Department of Chemical Engineering, University of Colorado, Boulder, Colorado 80309-0215, and Nanomaterials Research LLC, Longmont, Colorado 80501

Received March 28, 2003. Revised Manuscript Received June 2, 2003

Anodic alumina (AA) membranes are composed of highly uniform, nanometer-scale pores arranged in a hexagonal close-packed array. Depositing conformal films inside the nanopores is extremely difficult because the nanopores have an ultrahigh aspect ratio of $L/d \approx 10^3$. Atomic layer deposition (ALD) is a thin film growth technique that can deposit highly uniform films on high-aspect-ratio substrates with monolayer thickness control. In this study, AA membranes were coated with Al_2O_3 and ZnO ALD films and subsequently analyzed using cross-sectional scanning electron microscopy (SEM) and electron probe microanalysis (EPMA). SEM analysis of individual nanopores revealed that the AA membranes with nanopore diameters of $d = 65$ nm and lengths of $L = 50$ μm could be coated conformally by Al_2O_3 ALD using sufficient reactant exposure times. Zn concentration profiles measured by EPMA following ZnO ALD showed the progressive infiltration of the ZnO ALD into the nanopores with increasing exposure times for aspect ratios as high as $L/d \sim 5000$. Monte Carlo simulation of the experimental results assuming Knudsen diffusion accurately reproduced the experimental Zn concentration profiles and predicted the minimum ALD reactant exposures necessary to achieve conformal films. The Monte Carlo simulation also predicted that the diffusion-limited deposition will become reaction-limited given a sufficiently low ALD reaction probability. To test this idea, Fourier transform infrared absorption measurements were performed during the coating of the AA membranes by Al_2O_3 and SiO_2 ALD. The surface reactions during Al_2O_3 ALD have a relatively high reaction probability of $\sim 10^{-3}$. In contrast, the surface reactions during SiO_2 ALD have a very low reaction probability of $\sim 10^{-8}$. In agreement with the predictions, diffusion-limited behavior with a $t^{1/2}$ time dependence was observed during Al_2O_3 ALD. Reaction-limited behavior with a t^1 time dependence was observed during SiO_2 ALD.

I. Introduction

Nanoporous anodic alumina (AA) membranes are formed by the controlled electrochemical oxidation or anodization of aluminum metal in certain electrolytes.[1−5] The unique physical characteristics of these membranes make them ideally suited for many technological applications such as nanoscale templates,[6,7] chemical filters,[8] gas separation elements and membranes,[9,10] gas sensors,[11] and catalysts.[12,13] Each square centimeter of the AA film is permeated by 10^8−10^{11} highly uniform, nonintersecting, cylindrical nanometer-scale pores. These nanopores are aligned perpendicular to the membrane surface and are arranged approximately in a hexagonally close-packed array. By adjusting the anodization conditions, AA membranes can be synthesized with pore diameters ranging from $d = 4$ to 200 nm and pore lengths in the range of $L = 1$ to over 200 μm. Consequently, the AA nanopores may have aspect ratios as high as $L/d = 2.5 \times 10^4$. The development of AA membrane-based gas sensors depends critically on the ability to deposit uniform films of chemoresistive materials inside the nanopores. The ultrahigh aspect ratios of the AA membrane nanopores seriously challenge

* To whom correspondence should be addressed. Phone: 303-492-3398. Fax: 303-492-5894. E-mail: steven.george@colorado.edu.
[†] Department of Chemistry and Biochemistry, University of Colorado.
[‡] Department of Chemical Engineering, University of Colorado.
[§] Nanomaterials Research LLC.
[||] Current affiliation: Hewlett-Packard Company, Corvallis, Oregon 97330.

(1) Keller, F.; Hunter, M. S.; Robinson, D. L. *J. Electrochem. Soc.* **1953**, *100*, 411.
(2) O'Sullivan, J. P.; Wood, G. C. *Proc. R. Soc. London A* **1970**, *317*, 511.
(3) Masuda, H.; Hasegwa, F.; Ono, S. *J. Electrochem. Soc.* **1997**, *144*, L127.
(4) Thompson, G. E. *Thin Solid Films* **1997**, *297*, 192.
(5) Ba, L.; Li, W. S. *J. Phys. D: Appl. Phys.* **2000**, *33*, 2527.
(6) Masuda, H.; Satoh, M. *Jpn. J. Appl. Phys.* **1996**, *35*, L126.
(7) Routkevitch, D.; Bigioni, T.; Moskovits, M.; Xu, J. M. *J. Phys. Chem.* **1996**, *100*, 14037.
(8) Lee, S. B.; Mitchell, D. T.; Trofin, L.; Nevanen, T. K.; Soderlund, H.; Martin, C. R. *Science* **2002**, *296*, 2198.
(9) Mardilovich, P. P.; Govyadinov, A. N.; Mukhurov, N. I.; Rzhevskii, A. M.; Paterson, R. J. *Membrane Sci.* **1995**, *98*, 131.
(10) Itoh, N.; Kato, K.; Tsuji, T.; Hongo, M. *J. Membr. Sci.* **1996**, *117*, 189.
(11) Varghese, O. K.; Gong, D. W.; Paulose, M.; Ong, K. G.; Grimes, C. A.; Dickey, E. C. *J. Mater. Res.* **2002**, *17*, 1162.
(12) Patermarakis, G.; Pavlidou, C. *J. Catal.* **1994**, *147*, 140.
(13) Miller, D.; Moskovits, M. *J. Am. Chem. Soc.* **1989**, *111*, 9250.

10.1021/cm0303080 CCC: $25.00
Published on Web 08/14/2003

Table 1. Anodization Conditions and Resulting AA Membrane Parameters for Electrochemical Synthesis of Nanoporous AA Membranes

anodization conditions				AA membrane parameters	
electrolyte	potential (V)	temperature (°C)	charge density (C/cm^2)	pore diameter (nm)	film thickness (μm)
1.2 M H_2SO_4	20	2	100, 200	19	50, 100
3% $H_2C_2O_4$	50	12	100	46	50
3% $H_2C_2O_4$	70	12	100	65	50

conventional thin film deposition methods such as physical vapor deposition and chemical vapor deposition.

Atomic layer deposition (ALD) is a superb technique for coating high-aspect-ratio materials. ALD utilizes a binary sequence of self-limiting chemical reactions between gas-phase precursor molecules and a solid surface. A thin film of material can be deposited by repeating the binary reaction sequence in an ABAB... fashion where each AB cycle deposits approximately one monolayer of material.[14,15] The digital aspect of the ALD growth process allows precise control over the film thickness. Moreover, the self-limiting property of the ALD reactions yields excellent film uniformity and conformality. ALD has enabled the coating of a variety of porous media including powders,[16−18] tubular gas separation membranes,[19−21] porous silicon,[22] and anodic alumina.[23]

Nanoporous AA membranes are an ideal template for exploring thin film deposition in ultrahigh-aspect-ratio structures. In this study, Al_2O_3 and ZnO ALD films were deposited in nanoporous AA membranes with pore diameters of $d = 19-65$ nm and lengths of $L = 50-92$ μm using a viscous-flow ALD reactor. Al_2O_3 ALD is one of the most well-studied ALD processes[24−28] and serves as a model system for examining ALD in porous media. Cross sectional scanning electron microscopy (SEM) is used to verify that the Al_2O_3 ALD conformally coats the AA membranes given sufficiently long reactant exposure times. ZnO is a semiconducting oxide material with gas sensing applications[29,30] and ZnO ALD has also received much attention.[31−36] Cross sectional electron microprobe analysis (EPMA) is used to quantify the extent of ZnO ALD penetration into the AA membranes versus exposure time.

Additional investigations were performed in which Al_2O_3 and SiO_2 ALD films were deposited on a nanoporous AA membrane under high vacuum conditions. In these experiments, the surface chemistry during the film growth was monitored using in situ Fourier transform infrared (FTIR) absorption measurements. Because of the different reactive sticking coefficients for Al_2O_3 and SiO_2 ALD, these studies allowed the time-dependence of the ALD process to be evaluated under different rate-limiting conditions. The reactant diffusion and ALD film growth in nanoporous membranes was also modeled using Monte Carlo simulation. This computer modeling accurately described the ALD growth in the nanoporous AA membranes. The Monte Carlo simulations also predicted the experimental conditions necessary to achieve conformal ALD films over a wide range of aspect ratios.

II. Experimental Section

A. Electrochemical Synthesis of Nanoporous AA Membranes. Self-organized, nanoporous aluminum oxide films were produced by the electrochemical anodization of 99.99% pure Al substrates in acidic electrolytes in a 2-electrode cell.[2] The anodization voltage, current, and temperature were controlled to obtain the desired pore diameter and film thickness. The anodization conditions are given in Table 1. Prior to anodization, the surface of the aluminum was lithographically masked to define circular membranes with a diameter of 1 cm. Following anodization, the nanoporous alumina was firmly attached to the Al substrate by a dense alumina layer. An electrochemical technique was used to remove this layer and to lift the membranes off the Al substrate. The resulting membranes have uniform cylindrical pores that are open on both faces of the membrane. Scanning electron microscope (SEM) images of the top and side views of a typical nanoporous AA membrane with a pore diameter of 40 nm and a thickness of ~120 μm are presented in Figure 1.

B. Atomic Layer Deposition on Nanoporous AA Membranes. The nanoporous AA membranes were coated by Al_2O_3 ALD and ZnO ALD using a viscous-flow ALD reactor.[37] The surface reactions were performed at a temperature of 177 °C using nitrogen carrier gas at a mass flow rate of 200 sccm and a pressure of 1 Torr. The AA substrates were placed in the reactor with the long axes of the nanopores oriented perpen-

(14) George, S. M.; Ott, A. W.; Klaus, J. W. *J. Phys. Chem.* **1996**, *100*, 13121.
(15) Ritala, M.; Leskela, M. In *Handbook of Thin Film Materials*; Nalwa, H. S., Ed.; Academic Press: San Diego, CA, 2001.
(16) Ferguson, J. D.; Weimer, A. W.; George, S. M. *Thin Solid Films* **2000**, *371*, 95.
(17) Ferguson, J. D.; Weimer, A. W.; George, S. M. *Chem. Mater.* **2000**, *12*, 3472.
(18) Ferguson, J. D.; Weimer, A. W.; George, S. M. *Thin Solid Films* **2002**, *413*, 16.
(19) Ott, A. W.; Klaus, J. W.; Johnson, J. M.; George, S. M.; McCarley, K. C.; Way, J. D. *Chem. Mater.* **1997**, *9*, 707.
(20) Berland, B. S.; Gartland, I. P.; Ott, A. W.; George, S. M. *Chem. Mater.* **1998**, *10*, 3941.
(21) Cameron, M. A.; Gartland, I. P.; Smith, J. A.; Diaz, S. F.; George, S. M. *Langmuir* **2000**, *16*, 7435.
(22) Ducso, C.; Khanh, N. Q.; Horvath, Z.; Barsony, I.; Utriainen, M.; Lehto, S.; Nieminen, M.; Niinisto, L. *J. Electrochem. Soc.* **1996**, *143*, 683.
(23) Dillon, A. C.; Ott, A. W.; Way, J. D.; George, S. M. *Surf. Sci.* **1995**, *322*, 230.
(24) Ott, A. W.; Klaus, J. W.; Johnson, J. M.; George, S. M. *Thin Solid Films* **1997**, *292*, 135.
(25) Higashi, G. S.; Fleming, C. G. *Appl. Phys. Lett.* **1989**, *55*, 1963.
(26) Ritala, M.; Saloniemi, H.; Leskela, M.; Prohaska, T.; Friedbacher, G.; Grasserbauer, M. *Thin Solid Films* **1996**, *286*, 54.
(27) Ericsson, P.; Bengtsson, S.; Skarp, J. *Microelectron. Eng.* **1997**, *36*, 91.
(28) Matero, R.; Rahtu, A.; Ritala, M.; Leskela, M.; Sajavaara, T. *Thin Solid Films* **2000**, *368*, 1.
(29) Xu, J. Q.; Shun, Y. A.; Pan, Q. Y.; Qin, J. H. *Sens. Actuators B Chem.* **2000**, *66*, 161.
(30) Xu, J. Q.; Pan, Q. Y.; Shun, Y. A.; Tian, Z. Z. *Sens. Actuators B Chem.* **2000**, *66*, 277.
(31) Lujala, V.; Skarp, J.; Tammenmaa, M.; Suntola, T. *Appl. Surf. Sci.* **1994**, *82/83*, 34.
(32) Yamada, A.; Sang, B.; Konagai, M. *Appl. Surf. Sci.* **1997**, *112*, 216.
(33) Ott, A. W.; Chang, R. P. H. *Mater. Chem. Phys.* **1999**, *58*, 132.
(34) Yousfi, E. B.; Fouache, J.; Lincot, D. *Appl. Phys. Lett.* **2000**, *153*, 223.
(35) Jensen, J. M.; Oelkers, A. B.; Toivola, R.; Johnson, D. C.; Elam, J. W.; George, S. M. *Chem. Mater.* **2002**, *14*, 2276.
(36) Elam, J. W.; Sechrist, Z. A.; George, S. M. *Thin Solid Films* **2002**, *414*, 43.
(37) Elam, J. W.; Groner, M. D.; George, S. M. *Rev. Sci. Instrum.* **2002**, *73*, 2981.

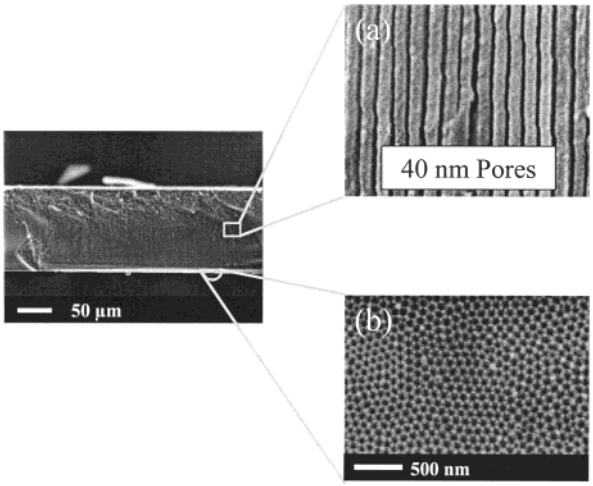

Figure 1. SEM images of uncoated AA membrane: (a) cross-sectional view of 40-nm diameter pores; (b) top view of hexagonal pore array.

dicular to the carrier gas flow. Rapid pressure changes might sweep the fragile AA membrane samples out of the flow tube. Consequently, care was taken to avoid rapid pressure changes during the depressurization following sample loading and the repressurization preceding sample unloading.

Alternating pulses of Akzo Nobel semiconductor grade trimethyl aluminum (TMA) and Fisher Optima purity deionized water were used for performing the Al_2O_3 ALD.[23−25] The A and B surface reactions that define the AB cycle for Al_2O_3 ALD are given by

$$AlOH^* + Al(CH_3)_3 \rightarrow AlOAl(CH_3)_2^* + CH_4 \quad (1)$$

$$AlCH_3^* + H_2O \rightarrow AlOH^* + CH_4 \quad (2)$$

where the asterisks designate the surface species. Similarly, Akzo Nobel semiconductor grade diethyl zinc (DEZ) and deionized water were used for depositing the ZnO ALD films.[31,33,34] The ZnO ALD occurred according to the binary reaction sequence

$$ZnOH^* + Zn(CH_2CH_3)_2 \rightarrow ZnOZn(CH_2CH_3)^* + C_2H_6 \quad (3)$$

$$Zn(CH_2CH_3)^* + H_2O \rightarrow ZnOH^* + C_2H_6 \quad (4)$$

The ALD reactant pulse timing sequence is given by: $t_1-t_2-t_3-t_4$ where the units are seconds and t_1 is the exposure time for reactant A, t_2 is the purge time following the A exposure, t_3 is the exposure time for reactant B, and t_4 is the purge time following the B exposure. ALD timing sequences ranging from 1−3−1−3 to 30−30−30−30 were employed to coat the nanoporous AA membranes. For the Al_2O_3 ALD exposures, a TMA partial pressure of 0.15 Torr was used, whereas for the ZnO ALD exposures a DEZ partial pressure of 0.068 Torr was used. The partial pressures used during the H_2O exposures were ∼2−3 times larger than the corresponding TMA and DEZ partial pressures.

The highest-aspect-ratio AA membranes required very large ALD reactant exposures. These large reactant exposures are impractical when using continuous flow in a viscous-flow reactor because they rapidly deplete the precursor reservoirs. Therefore, the viscous-flow ALD reactor was operated in a quasi-static mode for the highest-aspect-ratio membranes. A computer-controlled pneumatic exhaust valve was installed between the flow tube and the exhaust mechanical pump. During each cycle for ZnO ALD, the flow tube was first evacuated below 0.035 Torr. The exhaust valve was then closed and 5 Torr DEZ was introduced into the reactor. After a DEZ exposure time of 120 s, the exhaust valve was opened and the flow tube was evacuated below 0.035 Torr. A nitrogen purge flow of 200 sccm at a pressure of 1 Torr was then supplied for 240 s. The same sequence was repeated for the H_2O half cycle using an H_2O pressure of 5 Torr and an exposure time of 120 s. This process was repeated for each AB cycle during ZnO ALD.

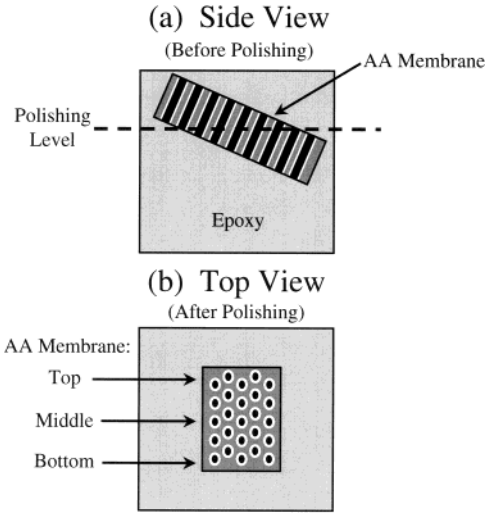

Figure 2. Illustration of polishing procedure to prepare coated AA membranes for cross-sectional SEM imaging: (a) side view of AA membrane in epoxy; (b) top view of AA membrane in epoxy after polishing.

C. Ex Situ Analysis of Coated Nanoporous AA Membranes. The nanoporous AA membranes coated by Al_2O_3 ALD were characterized using ex situ scanning electron microscopy (SEM) measurements. The AA membrane samples were prepared for SEM analysis by first embedding them in epoxy at a shallow angle as illustrated in Figure 2a. The epoxy stub was then polished with a progressively finer grit sandpaper to expose the cross-section of the membrane. The membrane sample was further polished using alumina polishing paste with a mean particle diameter of 40 nm. By mounting and polishing the AA membrane at a shallow angle, a cross sectional view of the nanopores was revealed as illustrated in Figure 2b. This procedure greatly facilitates SEM analysis because cross sections of the nanopores from different locations along the entire thickness of the AA membrane are prepared in a single plane.

Prior to imaging the polished AA membranes by SEM, the samples were etched briefly using phosphoric acid. This process improves the contrast between the Al_2O_3 ALD and the anodic Al_2O_3 and widens the nanopores in the uncoated regions of the membrane. These effects result from the greater chemical stability of Al_2O_3 ALD in phosphoric acid compared with that of the anodic alumina.[9] After the phosphoric acid etching treatment, the nanoporous AA membranes coated by Al_2O_3 ALD were examined using a JEOL JSM-5800 scanning electron microscope.

The SEM measurements provide a direct observation of the ALD films on the surfaces of the nanopores. This capability enables a qualitative assessment of the uniformity of the ALD coating along the length of the nanopores. However, quantifying the film thickness coverage profile from the SEM images is difficult. The quantified film thickness coverage profiles are necessary for comparing the experimental results with the Monte Carlo simulations. Consequently, electron probe microanalysis (EPMA) measurements were performed on the nanoporous AA membranes following ZnO ALD. These measurements allow a quantitative determination of the Zn concentration in the AA membranes versus distance into the pores. The EPMA measurements were performed by Prof. John Drexler of the Department of Geological Sciences at the University of Colorado.

Prior to the EPMA measurements, the nanoporous AA membranes coated by ZnO ALD were cleaved to expose an interior portion of the AA membrane. The samples were then

mounted in an epoxy stub with the long axes of the nanopores aligned parallel to the top face of the stub. The samples were polished and then coated with a thin carbon film to prevent sample charging during the EPMA measurements. The EPMA measurements employed a JEOL 8600 electron microprobe using an electron beam energy of 15 keV and a current of 20 nanoamps. Because the EPMA measurements have a spatial resolution of 3−5 μm, these measurements average over several hundred nanopores at a time.

D. In Situ Fourier Transform Infrared Studies. In situ Fourier transform infrared (FTIR) transmission measurements were conducted during the Al_2O_3 and SiO_2 ALD on a nanoporous AA membrane. The FTIR experiments were performed in a high-vacuum apparatus equipped with a Nicolet Magna 560 spectrometer and an MCT-B detector.[16−18] The sample substrate for the FTIR studies consisted of a nanoporous AA membrane with a pore diameter of $d = 47$ nm and a thickness of $L = 50$ μm. The AA membranes transmit infrared light and consequently the FTIR measurements monitor changes in surface species along the inner surfaces of the nanopores. The perimeter of the AA membrane was attached to a tungsten support grid using Aremco Ceramabond 571 ceramic adhesive. Tantalum metal foils spot-welded to each side of the tungsten grid allowed the sample to be held by copper clamps. The sample could be resistively heated by passing current through the tungsten grid and tantalum foils. The sample temperature was monitored by a chromel−alumel thermocouple that was attached to the bottom edge of the AA membrane with ceramic adhesive.

FTIR absorption measurements were performed versus time during sequential TMA and H_2O exposures to monitor the surface species on the AA membrane during Al_2O_3 ALD at 177 °C. Additional FTIR measurements were performed versus time during sequential $SiCl_4$ and H_2O exposures to monitor the surface species on the AA membrane during SiO_2 ALD at 427 °C. The SiO_2 ALD surface reactions proceed according to[38,39]

$$SiOH^* + SiCl_4 \rightarrow SiOSiCl_3^* + HCl \quad (5)$$

$$SiCl^* + H_2O \rightarrow SiOH^* + HCl \quad (6)$$

The SiO_2 ALD experiments used $SiCl_4$ (purity 99.999%) obtained from Alfa Aesar.

III. Results

A. Scanning Electron Microscopy Following Al_2O_3 ALD. Nanoporous AA membranes with dimensions of $d = 65$ nm and $L = 50$ μm were coated using 100 AB cycles for Al_2O_3 ALD at a deposition temperature of 177 °C. Four different experiments were performed using ALD timing sequences of 1−5−1−5, 3−6−3−6, 10−30−10−30, and 30−30−30−30. On a flat surface, these deposition conditions would yield an Al_2O_3 film thickness of 129 Å.[36] If the Al_2O_3 ALD deposits at the same growth rate in the nanoporous AA membranes, the pore diameter d should be reduced from 65 to 39 nm. Figure 3 shows the SEM images recorded from the top, middle, and bottom portions of the AA membranes. The top and bottom images show the similar degree of ALD coating for all of the exposure times. This behavior is expected because the top and bottom of the AA membrane are directly exposed to the ALD reactant precursors in the flow tube. Consequently, no diffusion of the reactant precursors is necessary to coat the top and bottom portions of the AA membranes. Reactant exposure times as short as 1 s should coat these regions.

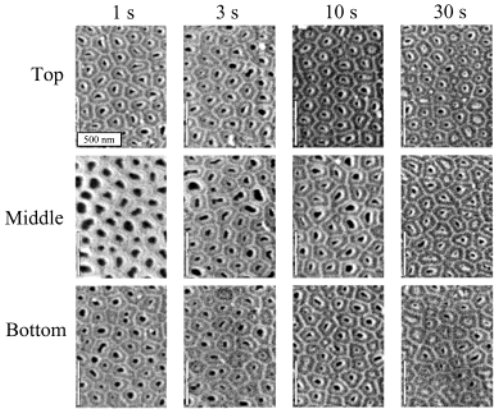

Figure 3. SEM images recorded from top, middle, and bottom portions of AA membranes following 100 AB cycles of Al_2O_3 ALD using exposure times of 1, 3, 10, and 30 s.

For the 1-s exposures in the middle portion of the membrane, the nanopores have been widened by the phosphoric acid etching process. These findings indicate that the 1-s exposures were insufficient for the Al_2O_3 ALD precursors to reach the middle of the 50-μm-long nanopores. In contrast, Figure 3 indicates that exposure times ≥3 s are sufficient to allow the Al_2O_3 ALD reactants to diffuse to the middle of the pores. Some of the pores in the middle portions of the samples for 3- and 10-s exposures are wider than average. These wider pores are attributed to increased etching by phosphoric acid resulting from less Al_2O_3 ALD. The gas conductance in these pores may have originally been less than the gas conductance in the surrounding pores.

B. Electron Probe Microanalysis Following ZnO ALD. Nanoporous AA membranes coated by ZnO ALD were analyzed using EPMA measurements. These measurements quantified the extent of infiltration of the ZnO ALD into the nanoporous membranes. AA membranes with dimensions of $d = 65$ nm and $L = 50$ μm were coated using 64 cycles for ZnO ALD at a deposition temperature of 177 °C. Four AA membrane samples were coated in separate experiments using ALD timing sequences of 1−5−1−5, 3−6−3−6, 10−30−10−30, and 30−30−30−30. These growth conditions yield a ZnO film thickness of 129 Å on a flat surface.[36] This ZnO ALD film should reduce the nanopore diameter from 65 to 39 nm.

Figure 4 shows two-dimensional EPMA dot maps in which the density of white spots represents the concentration of Zn atoms. In each of the images in Figure 4, the Zn concentration is high near the top and bottom surfaces of the AA membrane. In addition, the Zn concentration extends progressively into the center of the membrane with increasing ZnO ALD exposure time. For the image recorded using exposure times of 30 s, the Zn concentration is nearly uniform. This finding is consistent with a conformal ZnO ALD film that is continuous along the entire length of the nanopore.

The distribution of Zn in the nanoporous AA membranes was quantified using EPMA line scans. In these measurements, the electron beam was scanned linearly across the AA membrane in the direction of the long axis of the nanopores while the Zn concentration was recorded in ~1-μm increments. The resulting Zn con-

(38) Sneh, O.; Wise, M. L.; Ott, A. W.; Okada, L. A.; George, S. M. *Surf. Sci.* **1995**, *334*, 135.
(39) Klaus, J. W.; Ott, A. W.; Johnson, J. M.; George, S. M. *Appl. Phys. Lett.* **1997**, *70*, 1092.

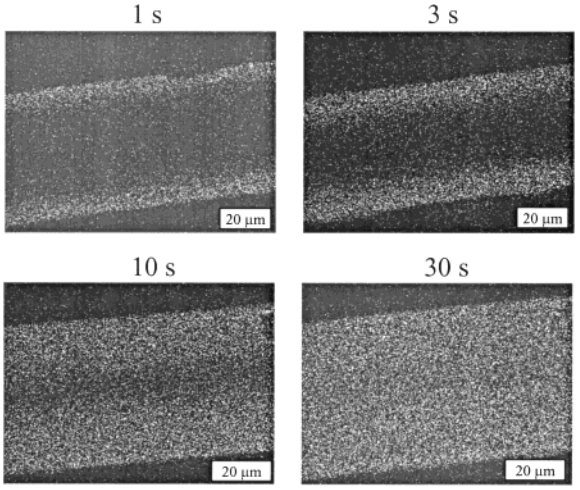

Figure 4. Cross-sectional elemental distribution map of Zn in AA membranes measured by EPMA following 64 AB cycles of ZnO ALD using exposure times of 1, 3, 10, and 30 s.

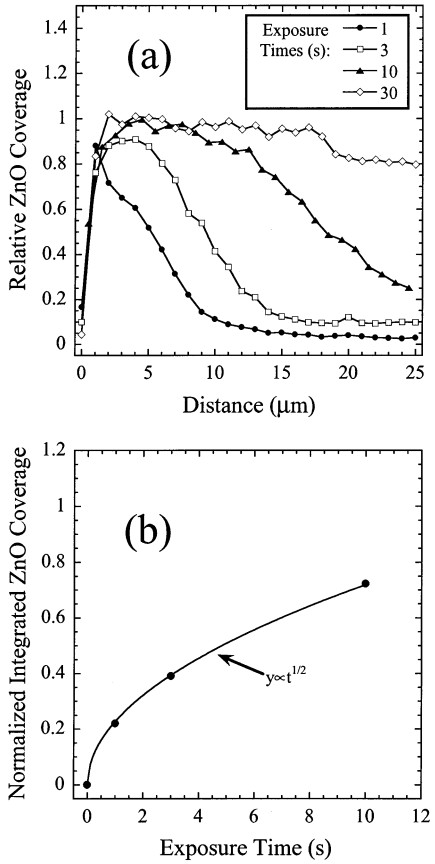

Figure 5. (a) Relative ZnO coverage measured by EPMA line scan and (b) normalized integrated ZnO coverage following 64 AB cycles of ZnO ALD using exposure times of 1, 3, 10, and 30 s.

centration measurements are presented in Figure 5a. In this figure, the Zn profiles have been normalized to the maximum measured Zn concentration. Figure 5a demonstrates that the ZnO ALD film extends farther into the AA membrane with increasing exposure time. For ZnO ALD exposure times of 30 s, the Zn concentration profile is nearly uniform throughout the nanoporous membrane to within ±10%.

Figure 5b plots the normalized integrated coverages of the ZnO profiles shown in Figure 5a. The solid line

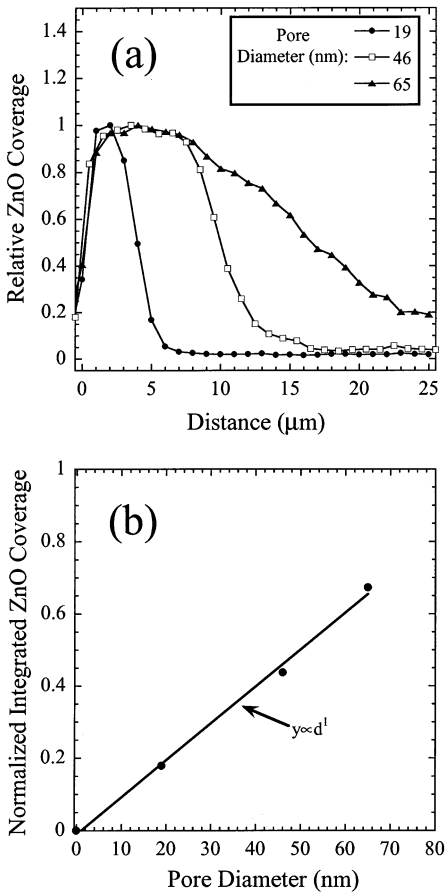

Figure 6. (a) Relative ZnO coverage measured by EPMA line scan and (b) normalized integrated ZnO coverage for AA membranes with pore diameters of 19, 46, and 65 nm following 19, 45, and 64 AB cycles, respectively, of ZnO ALD using exposure times of 5 s.

in Figure 5b shows a least-squares fit to the integrated ZnO coverages between 0 and 10 s using the functional form $y = kt^{1/2}$. This fit indicates that the integrated ZnO coverage obeys a $t^{1/2}$ time dependence before approaching the limiting saturation ZnO coverage at ZnO ALD exposure times of $t > 10$ s.

Additional experiments investigated the effect of the diameter of the nanopores on the resulting ZnO ALD coverage profile. AA membranes with $L = 50$ μm and pore diameters of $d = 19$, 46, and 65 nm were coated in separate experiments using 19, 45, and 64 AB cycles for ZnO ALD, respectively. The number of AB cycles was chosen to reduce the pore diameter by ~40% in each case. These experiments used a ZnO ALD timing sequence of 5−10−5−10 and a deposition temperature of 177 °C. Figure 6a demonstrates that the ZnO ALD profiles extend farther into the nanopores with increasing pore diameter when the exposure times are held constant at 5 s. This effect is quantified by the normalized integrated ZnO coverages shown in Figure 6b. The solid line in Figure 6b is a linear least-squares fit to the integrated ZnO coverage measurements.

A final ZnO ALD coating experiment was performed on a nanoporous AA membrane with an extremely high aspect ratio. This AA membrane had dimensions $d = 19$ nm and $L = 92$ μm yielding an aspect ratio $L/d \approx 5000$. To coat these ultrahigh-aspect-ratio nanopores, the viscous-flow ALD reactor was operated in a quasi-static mode as described in Section II. B. The membrane

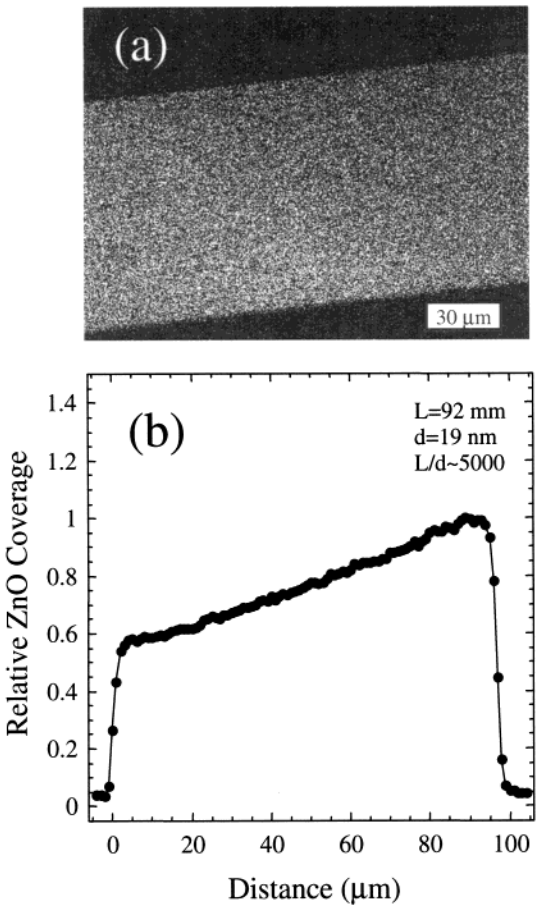

Figure 7. (a) Zn elemental distribution map measured by EPMA and (b) relative ZnO coverage for AA membrane with an aspect ratio $L/d \approx 5000$ following 19 AB cycles of ZnO ALD.

was coated using 19 ZnO ALD cycles with exposure times of 120 s and reactant pressures of 5 Torr at a deposition temperature of 177 °C. The resulting EPMA dot map and ZnO concentration profile are presented in Figures 7a and b, respectively. The absence of a dip near 50 μm in Figure 7b indicates that the ZnO ALD coating is continuous through the nanopores. The slope exhibited by the ZnO concentration profile may result from the orientation of the sample during EPMA. The slope may also be caused either by a slight gradient of the pore diameter or incomplete opening of the pores during the separation of AA films from the Al substrates. Both of these conditions would lead to a gradient in the ZnO concentration.

C. Fourier Transform Infrared Measurements During Al_2O_3 and SiO_2 ALD. The TMA and H_2O half reactions for Al_2O_3 ALD require saturation exposures of $\sim 10^4$ L.[24] The exposure unit of 1 Langmuir (L) is equal to 1×10^{-6} Torr s. In contrast, the $SiCl_4$ and H_2O half reactions for SiO_2 ALD require much larger exposures of $\sim 10^9$ L to achieve saturation.[39] These results imply that TMA and H_2O have much higher reactive sticking coefficients on the Al_2O_3 ALD surface compared with the reactive sticking coefficients for $SiCl_4$ and H_2O on the SiO_2 ALD surface. To explore the effect of the reactive sticking coefficient on the ALD coating of nanoporous AA membranes, in situ Fourier transform infrared (FTIR) measurements were performed during Al_2O_3 and SiO_2 ALD.

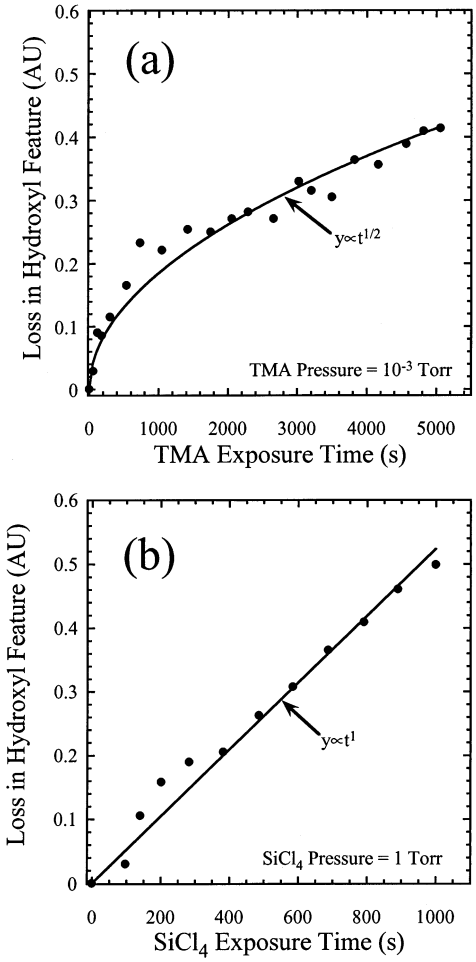

Figure 8. Loss in hydroxyl feature measured by FTIR spectroscopy during (a) Al_2O_3 ALD versus TMA exposure time and (b) SiO_2 ALD versus $SiCl_4$ exposure time.

A nanoporous AA membrane with dimensions of $d =$ 47 nm and $L = 50$ μm was used for the FTIR studies. After installing the nanoporous AA membrane in the high-vacuum FTIR chamber, an initial Al_2O_3 ALD layer was deposited on the membrane. This Al_2O_3 ALD layer was deposited using 4 TMA/H_2O cycles with reactant pressures of 2−5 Torr and exposure times of 15−30 min at a substrate temperature of 177 °C. FTIR measurements confirmed that these exposures were sufficient to saturate the individual ALD half reactions. After depositing the initial Al_2O_3 ALD layer, the FTIR spectrum of the nanoporous AA membrane exhibited a broad absorption between $\sim$2700−3800 cm^{-1} attributed to the O−H stretching vibrations of the AlOH* surface hydroxyl species.[23]

The hydroxyl-terminated Al_2O_3 surface was then subjected to successive, small TMA exposures at a substrate temperature of 177 °C using a TMA pressure of $\sim 1 \times 10^{-3}$ Torr and various exposure times. Following each TMA exposure, the FTIR spectrum of the nanoporous AA sample was recorded at 77 °C. The intensity of the AlOH* FTIR feature was observed to decrease with increasing TMA exposure as predicted by eq 1. The loss of integrated absorbance for the AlOH* feature versus TMA exposure is shown in Figure 8a. The solid line in Figure 8a shows a nonlinear least-squares fit to the FTIR data using the function $y = kt^{1/2}$ where k is a fitting constant.

Additional FTIR experiments were performed during SiO_2 ALD. Prior to these measurements, the Al_2O_3 ALD surface was converted to an SiO_2 ALD surface using 2 $SiCl_4/H_2O$ cycles for SiO_2 ALD. These exposures used $SiCl_4$ and H_2O pressures of 10 Torr and exposure times of 5 min at 427 °C. Following this procedure, FTIR measurements revealed a relatively sharp absorption at $\sim$3740 cm^{-1} attributed to the O−H stretching vibration of the SiOH* surface hydroxyl species.[38]

The hydroxyl-terminated SiO_2 surface was subjected to progressive $SiCl_4$ exposures using a $SiCl_4$ pressure of $\sim$1 Torr and various exposure times at 427 °C. Following each $SiCl_4$ exposure, the FTIR spectrum of the nanoporous AA surface was recorded at 77 °C. The integrated absorption of the SiOH* FTIR feature decreased with $SiCl_4$ exposure in agreement with eq 5. Figure 8b plots the loss of integrated absorbance for the SiOH* feature versus $SiCl_4$ exposure. The solid line in Figure 8b presents a linear least-squares fit to the FTIR data.

IV. Discussion

The SEM and EPMA measurements in Figures 3−7 clearly show that the ZnO and Al_2O_3 ALD coating of the nanoporous AA membranes is dictated by a diffusional process. The ends of the nanopores are coated immediately using short reactant exposures, while progressively longer reactant exposure times are required to coat the positions inside the nanopores. The infiltration of the ZnO ALD into the nanopores increases with both reactant exposure time and pore diameter. To quantify the experimental results and also to predict the reactant exposures necessary to achieve conformal coating, a Monte Carlo computer simulation was developed. This simulation assumes that molecular transport occurs by Knudsen diffusion and that coating occurs by self-limiting adsorption. In addition, this model accounts for the pore size reduction with increasing numbers of ALD cycles.

A. Monte Carlo Simulation of ALD in Nanoporous AA Membranes. One of the assumptions made in this model is that transport through the nanopores occurs via molecular flow. This assumption is reasonable because the mean free path of the ALD reactant molecules greatly exceeds the diameter of the nanopores. For example, the mean free path of TMA in 1 Torr N_2 at 450 K is $\lambda \approx 4 \times 10^{-5}$ m while the AA membranes have diameters $d \approx 1 \times 10^{-7}$ m. Second, only the A half reaction (TMA or DEZ) of each AB cycle was considered in the simulations. This simplification is justified because the TMA and DEZ molecules are heavier and diffuse more slowly than H_2O. The H_2O pressures used during the ZnO and Al_2O_3 ALD AB cycles were also typically $\sim$2−3 times larger than the corresponding DEZ and TMA pressures. Assuming comparable reactive sticking coefficients during the A and B half reactions, the slower diffusion and lower pressures during the TMA and DEZ exposures argue that the A half reaction will be rate-limiting.

All of the nanopores in a given AA membrane are assumed to be identical and to have cylindrical symmetry. Furthermore, particles enter from both ends of the pores at equal rates. These assumptions allow the AA membrane to be represented by a 1-dimensional array with a length of $L/2$ in which each element in the array records the diameter of the nanopore at a specific distance from the entrance of the tube. The diameter of a given segment of the nanopore decreases as that segment becomes coated by the ALD film. The number of elements in the array is typically 20−100. This number is much smaller than the actual number of reactive surface sites on the nanopore. Consequently, each element in the array represents a large number of reactive surface sites.

The Monte Carlo simulation follows the trajectory of individual molecules as they diffuse in the nanopore. Initially, the molecule is located at the pore entrance. The trajectory progresses in discrete steps during which the molecule moves a distance $\pm d_i$ where d_i is the diameter of the nanopore in the ith element of the array at the current location of the molecule. According to the theory of Knudsen diffusion, d_i is the average distance traveled by a gas molecule under molecular flow in a tube having a diameter d_i.[40] This average distance is much smaller than the length of the elements in the array. Exact positions are recorded for the molecule during its diffusion in each element of the array.

Simulating the diffusion as discrete steps of $\pm d_i$ in the 1-dimensional array is formally equivalent to following individual trajectories in 3 dimensions. These discrete steps in the 1-dimensional array characterize the molecules desorbing from the cylindrical tube wall in a $\cos(\theta)$ distribution with respect to the surface normal and isotropically in azimuthal angle around the surface normal. At each step in the trajectory, the direction of the motion is selected randomly where $+d_i$ represents motion into the nanopore and $-d_i$ represents motion out of the nanopore. After moving the distance $\pm d_i$, the molecule may transfer to a new array element. If the molecule moves beyond the last array element at $L/2$, the direction of the trajectory is reversed and the molecule is reflected back into the tube. This simplification accounts for molecules that arrive from the opposite end of the tube. This model may overestimate the rate of diffusion through the nanopores because molecules desorbing at large θ may experience gas-phase collisions.

After each trajectory step, a random number, R, is chosen between 0 and 1. If $R < S$, where S is the ALD reactive sticking coefficient, and if the occupied array element has not yet reacted during the current ALD cycle, then the diameter of the occupied array element, d_i, is reduced by $2G$ where G is the ALD growth rate. During each AB cycle of the simulation, each element in the array may react only once. This constraint models the self-limiting nature of ALD growth. The trajectory continues until the molecule reacts or exits the nanopore. The number of trajectories simulated during each AB cycle is chosen to model accurately the experimental ALD exposures. In addition, the number of simulated AB cycles is equal to the number of AB cycles used in the experiment.

To model accurately the experimental ALD exposures, the amount of time represented by one trajectory is calculated from $t = N/(\Phi A)$ where N is the number of molecules represented by one trajectory and ΦA is the

(40) Present, R. D. *Kinetic Theory of Gases*; McGraw-Hill Book Company, Inc.: New York, 1958.

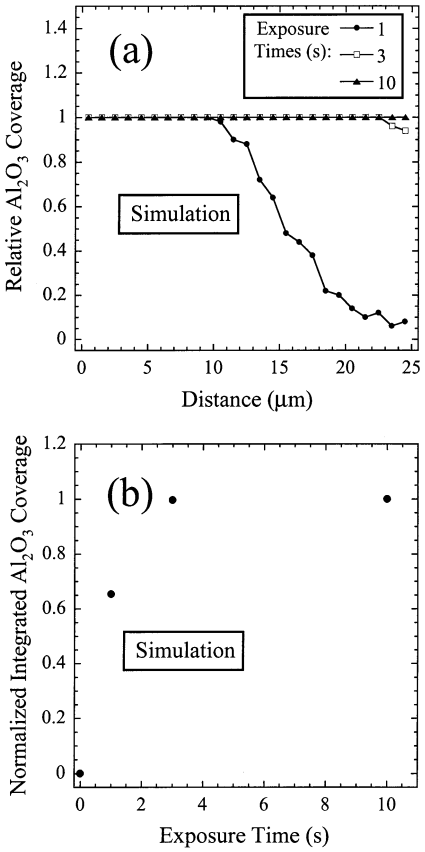

Figure 9. (a) Simulated Al_2O_3 coverage profiles versus distance into nanopore and (b) normalized integrated Al_2O_3 coverages for TMA exposure times of 1, 3, and 10 s.

number of molecules entering the nanopore in one second. The nanopore is represented by an array with 20−100 elements. When a trajectory terminates with a reaction, all of the surface sites represented by the occupied array element are coated simultaneously. Consequently, the number of molecules represented by one trajectory is $N = (\alpha\gamma)/x$ where α is the surface area of the nanopore, γ is the areal density of reactive sites in units of sites cm^{-2}, and x is the number of array elements. The surface area of a nanopore with a length of $^L/_2$ is $\alpha = R\pi dL/2$ where $R = 1.5$ is a surface area roughness factor determined experimentally for the nanoporous AA membranes. The areal density of reactive sites is calculated from the density of the film and the ALD growth rate. For Al_2O_3 ALD in a nanopore with $d = 65$ nm, $L = 50$ μm, and $x = 50$, $N = 7.0 \times 10^5$ molecules.

The number of molecules/s entering the nanopore is given by ΦA where Φ is the flux of reactant molecules and A is the cross-sectional area of the nanopore. The flux of reactant molecules is $\Phi = p/(2\pi mkT)^{1/2}$ where p is partial pressure, m is molecular weight, and T is temperature. The cross-sectional area of the nanopores is $A = \pi d^2/4$. Assuming a TMA partial pressure of 0.15 Torr at 177 °C and using $d = 65$ nm, $\Phi A = 9.7 \times 10^8$ molecules/s. Therefore, the amount of time represented by one trajectory is $N/(\Phi A) = 7.2 \times 10^{-4}$ s. Conversely, the number of trajectories required to simulate an ALD exposure time of 1 s at a TMA partial pressure of 0.15 Torr is: $(\Phi A)/N = 1.4 \times 10^3$.

B. Simulated Al_2O_3 ALD Coating of Nanopores. Figure 9a shows the thickness profiles resulting from the Monte Carlo simulation for a nanoporous AA membrane having $d = 65$ nm and $L = 50$ μm following 100 Al_2O_3 ALD cycles. The reactive sticking coefficient for Al_2O_3 ALD was $S = 1 \times 10^{-3}$. These simulations used the same TMA pressure and exposure times as the experiments in Figure 3. Figure 9a demonstrates that 1-s reactant exposures yield a uniform Al_2O_3 ALD coverage for the first ~11 μm into the nanopore. Beyond ~11 μm, the relative thickness of the coating decreases with distance into the nanopore. At a distance of 25 μm, the relative Al_2O_3 coverage is only ~0.05−0.1.

Using 3-s reactant exposures, Figure 9a shows that the relative thickness of the Al_2O_3 ALD coating is nearly uniform throughout the nanopore and decreases only slightly to ~0.95 at 25 μm. The relative Al_2O_3 coverage is completely uniform for reactant exposure times ≥10 s. Figure 9b shows the simulated normalized integrated Al_2O_3 coverage profiles. The simulations predict that the normalized integrated coverage is nearly constant at 1.0 for reactant exposure times ≥3 s.

The Monte Carlo results in Figure 9 correspond very well with the SEM measurements in Figure 3. The experimental SEM results in Figure 3 demonstrate that the middle portion of the $d = 65$ nm, $L = 50$ μm AA membrane is not coated using reactant exposure times of 1 s. The simulated Al_2O_3 coverage profile using exposure times of 1 s in Figure 9a shows a relative Al_2O_3 coverage of only ~0.05−0.1 at a distance of 25 μm. This translates to a predicted thickness for the Al_2O_3 ALD coating of ~6−13 Å. This low coverage is probably insufficient to protect the walls of the nanoporous AA membrane during the phosphoric acid etch procedure.

C. Simulated ZnO ALD Coating of Nanopores. Figure 10 shows the simulated ZnO coverage profiles for a nanopore with $d = 65$ nm and $L = 50$ μm using reactant exposure times of 1, 3, 10, and 30 s. These simulations used 64 ZnO ALD cycles under conditions similar to those of the experiments shown in Figures 4 and 5. The reactive sticking coefficient for ZnO ALD was $S = 7 \times 10^{-3}$. The simulated ZnO coverage profiles in Figure 10a closely match the experimental measurements in Figure 5a. Figure 10a predicts that the nanopores should be coated conformally using ~30-s reactant exposures. The open diamonds in Figure 5a show that the nanopores are coated very evenly using reactant exposures of 30 s. The slight drop in relative coverage at 20−25 μm may result from nonidealities in the AA structure such as sections with reduced diameter or blocked pores.

Figure 10b shows the normalized integrated ZnO coverages from the simulated coverage profiles in Figure 10a versus reactant exposure time. These data agree very well with the experimental measurements in Figure 5b. The solid line in Figure 10b results from a nonlinear least-squares fit to the function $y = kt^{1/2}$ with $k = 0.28$. A similar fit to the experimental data in Figure 5b yielded $y = kt^{1/2}$ with $k = 0.23$.

The Monte Carlo simulation was also used to model the influence of the nanopore tube diameter on the ZnO ALD coverage profiles. Figure 11a plots the simulated relative ZnO coverage profiles for 5-s reactant exposures in nanopores with $L = 50$ μm and $d = 19$, 47, and 65 nm. The integrated coverages are shown in Figure 11b. The linear least-squares fit in Figure 11b yields a slope

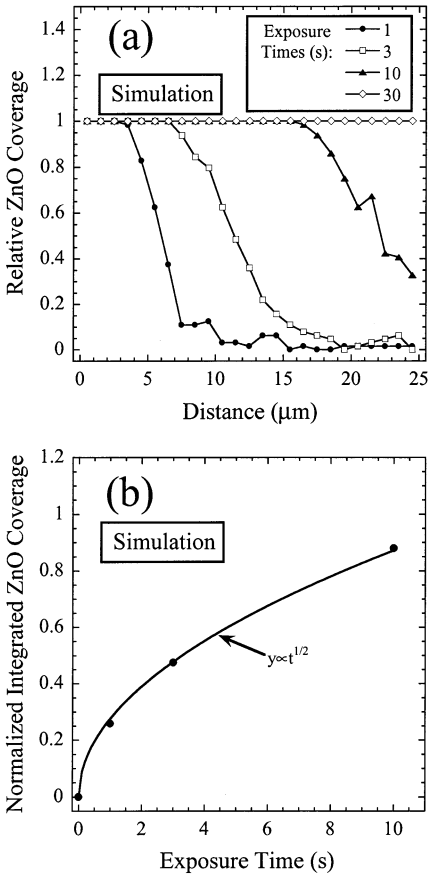

Figure 10. (a) Simulated ZnO coverage profiles versus distance into nanopore and (b) normalized integrated ZnO coverages for DEZ exposure times of 1, 3, 10, and 30 s.

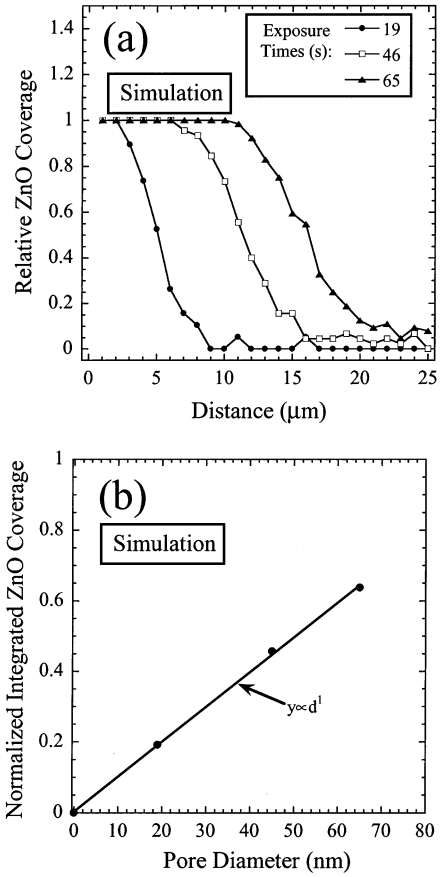

Figure 11. (a) Simulated ZnO coverage profiles versus distance into nanopore and (b) normalized integrated ZnO coverages for nanopore diameters of 19, 46, and 65 nm using DEZ exposure times of 5 s.

of 0.25 integrated ZnO coverage units per nm. The simulations in Figure 11 agree very well with the experimental results in Figure 6. In particular, the linear least-squares fits to the integrated ZnO coverages in Figures 6b and 11b both yield a slope of 0.25 integrated ZnO coverage units per nm.

D. Diffusion-Limited and Reaction-Limited Regimes. The ALD coating of nanoporous AA membranes can be either diffusion- or reaction-limited depending on the reactive sticking coefficient and the nanopore aspect ratio. These two kinetic regimes yield different coverage profiles. This process can be described by

$$A \xrightarrow[\text{diffusion}]{H} B \xrightarrow[\text{reaction}]{S} C \qquad (7)$$

where A represents a molecule that has entered the nanopore, B represents a molecule that has diffused to an empty site, and C represents a molecule that has reacted. The reaction rate is quantified by S, the reactive sticking coefficient. S is the probability that a surface collision results in reaction and can be determined from reactive uptake measurements.

The diffusion rate can be quantified by H, the "hopping coefficient". H is the probability that a given hop reaches an empty site. H can be calculated from a 1-dimensional random walk analysis.[41] The most probable number of hops required to reach a site located a net distance of j hops away from the starting point is j^2. Therefore, the probability that a given hop reaches this empty site is $H = 1/j^2$. An average distance to an empty site is taken to be $L/4$, i.e., halfway to the midpoint of the 1-dimensional array. Dividing this distance by the average hop length, d,[40] yields $j = L/(4d)$. The resulting hopping coefficient is $H = 1/j^2 = 16(d/L)^2$

The diffusion-limited kinetic regime occurs when $S \gg H$. Monte Carlo simulations in this regime reveal that the sites fill approximately in order from the entrance of the tube. In addition, the simulated coverage profiles versus exposure time exhibit a relatively distinct boundary between the coated and uncoated regions as shown in Figure 10a. Simulations performed in the diffusion-limited regime are independent of the sticking coefficient when $S \gg H$. In contrast, simulations performed in the reaction-limited regime with $S \ll H$ show the sites fill randomly yielding relatively flat coverage profiles. These results demonstrate that when $S \ll H$, the reactant molecules will equilibrate nearly completely throughout the AA membrane before reacting.

Figure 12a predicts that the integrated coverage versus time in the diffusion-limited regime has a $t^{1/2}$ time dependence. Figure 12a results from a simulation using $d = 65$ nm, $L = 50$ μm, and $S = 7 \times 10^{-3}$. The hopping coefficient is $H = 2.7 \times 10^{-5}$ and $S \gg H$. In contrast, the reaction-limited case in Figure 12b shows a t^1 time dependence. For convenience, the simulation in Figure 12b used $d = 65$ nm, $L = 0.5$ μm, and $S = 1 \times 10^{-4}$. The hopping coefficient is $H = 2.7 \times 10^{-1}$ and $S \ll H$ for the much thinner AA membrane with $L =$

(41) Atkins, P. W. *Physical Chemistry*; W. H. Freeman and Company: New York, 1986.

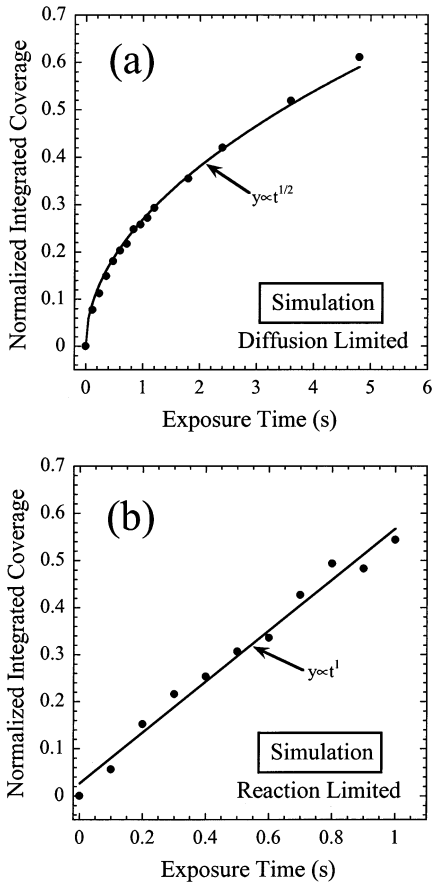

Figure 12. Normalized integrated coverages versus exposure time simulated using (a) diffusion-limited and (b) reaction-limited conditions. Plot (a) for $S \gg H$ uses $d = 65$ nm, $L = 50$ μm, $S = 7 \times 10^{-3}$, and $H = 2.7 \times 10^{-5}$. Plot (b) for $S \ll H$ uses $d = 65$ nm, $L = 0.5$ μm, $S = 1 \times 10^{-4}$, and $H = 2.7 \times 10^{-1}$.

0.5 μm. Figures 12a and 12b both model ZnO ALD assuming a DEZ pressure of 0.068 Torr in the low coverage limit. The simulations yield normalized integrated coverages of 1 following long exposures for both kinetic regimes.

The time-dependent coverages predicted for the diffusion- and reaction-limited regimes were observed experimentally. Figure 8a shows the loss in hydroxyl feature observed using the FTIR measurements during one TMA exposure. This experiment was performed using a nanoporous substrate with $d = 47$ nm and $L = 50$ μm yielding $H = 1.4 \times 10^{-5}$. The reactive sticking coefficient during Al_2O_3 ALD is $S \approx 1 \times 10^{-3}$ [ref 24] and $S \gg H$. In agreement with the simulations in Figure 12a, Figure 8a exhibits a $t^{1/2}$ time dependence.

The FTIR measurements in Figure 8b show the decrease in hydroxyl coverage versus $SiCl_4$ exposure during one AB cycle of SiO_2 ALD. These experiments employed the same nanoporous substrate as in Figure 8a with $H = 1.4 \times 10^{-5}$. The reactive sticking coefficient during SiO_2 ALD is S $\approx 10^{-8}$ [ref 39] and $S \ll H$. In agreement with the simulations in Figure 12b, Figure 8b exhibits a t^1 time dependence.

In the diffusion-limited regime when $S \gg H$, the results from the Monte Carlo simulations are insensitive to the choice of reactive sticking coefficient, S. There is good agreement between the Monte Carlo results in Figures 9, 10, and 11 and the corresponding experimental results in Figures 3, 5, and 6. This agreement is obtained without any adjustable fitting parameters when the reactive sticking coefficient is much greater than the hopping coefficient, i.e., $S \gg H$.

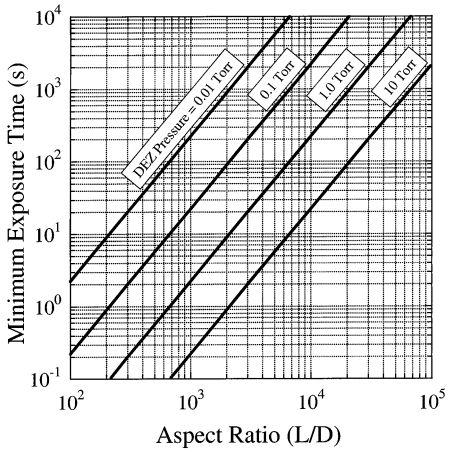

Figure 13. Predicted minimum exposure times to achieve conformal ZnO ALD in AA membranes versus aspect ratio assuming DEZ pressures of 0.01, 0.1, 1, and 10 Torr.

E. Predicted Minimum Exposure Times. The Monte Carlo simulations can be utilized to determine the minimum exposure times for conformal deposition on high-aspect-ratio pores. These predictions are valid in the limit that $S \gg H$, i.e., the reactive sticking coefficient, S, is much greater than the hopping coefficient, H. These simulations are general and applicable to various ALD surface chemistries. The hopping coefficient depends only on the aspect ratio of the substrate, viz. $H = 16(d/L)^2$.

On the basis of the Monte Carlo simulations, the integrated coverage, Θ^*, was empirically found to obey the following expression in the diffusion-limited regime:

$$\Theta^* = kt^{1/2} \tag{8}$$

In this expression, Θ^* is the integrated coverage, t is the exposure time, and k is a parameter that depends on reactant pressure, reactant mass, and the density of ALD reactive sites. The k parameter can be written as

$$k = 2.1 \times 10^3 P^{1/2}\, m^{-1/4}\, \Gamma^{-1/2}\, (L/d)^{-1} \tag{9}$$

where k has units of $t^{-1/2}$ and t is in seconds. In addition, P is the reactant pressure in Torr, m is the mass of the reactant molecule in amu, and Γ is the density of ALD reactive sites in 10^{15} cm^{-2}.

The minimum time required to achieve a saturation exposure can be determined by setting $\Theta^* = 1$ in eq 8. Subsequently, eqs 8 and 9 can be solved for the required exposure time to coat pores conformally when $S \gg H$

$$t = 2.3 \times 10^{-7} P^{-1}\, m^{1/2}\, \Gamma\, (L/d)^2 \tag{10}$$

For example, for $P = 5$, $L/d = 5000$, $m = 123$ for DEZ, and $\Gamma = 0.84$, eq 10 predicts a minimum exposure time of $t = 11$ s for a conformal coating. Equation 10 should have great utility for predicting the required exposure time for coating ultrahigh-aspect-ratio porous samples.

Figure 13 plots the required exposure time versus aspect ratio from eq 10 for ZnO ALD assuming DEZ pressures of 0.01, 0.1, 1.0, and 10 Torr. Figure 13 reveals that ultrahigh aspect ratios of 10^3−10^4 can be coated

conformally with reactant pressures of 1−10 Torr in exposure times of 1−10 s. These experimental conditions can be easily implemented for ZnO ALD. Consequently, the ALD exposure times required to coat ultrahigh-aspect-ratio porous samples are not prohibitively long. The results of Figure 13 can be generalized to other ALD surface chemistries by employing the appropriate values for m and Γ in eq 10.

V. Conclusions

Atomic layer deposition was demonstrated on ultrahigh-aspect-ratio nanopores of anodic alumina (AA). SEM cross-sectional analysis revealed that AA membranes with nanopore dimensions of $d = 65$ nm and $L = 50$ μm could be coated conformally by Al_2O_3 ALD using sufficient reactant exposure times. Zn concentration profiles measured using EPMA following ZnO ALD of AA membranes revealed the progressive infiltration of Zn into the nanopores with increasing exposure times for aspect ratios as high as $L/d \sim 5000$. Monte Carlo simulations of these experiments accurately reproduced the experimental Zn concentration profiles. Furthermore, this modeling predicted that the diffusion-limited coating process would become reaction-limited given a sufficiently low ALD reaction probability. In agreement with these predictions, in situ FTIR measurements revealed that diffusion-limited behavior with a $t^{1/2}$ time dependence was observed for the rapid $AlOH^* + Al(CH_3)_3 \rightarrow AlOAl(CH_3)_2^* + CH_4$ reaction during Al_2O_3 ALD. Reaction-limited behavior with a t^1 time dependence was observed for the $SiOH^* + SiCl_4 \rightarrow SiOSiCl_3^* + HCl$ reaction during SiO_2 ALD. The Monte Carlo simulations predict the minimum ALD exposures required to achieve conformal coverage on nanopores over a wide range of aspect ratios. These predictions are very general and should have utility for determining the required exposures for conformal ALD coating on porous substrates.

Acknowledgment. This research was funded by Nanomaterials Research LLC as part of the Department of Energy SBIR Project DE-FG03 00 ER83053. Additional funding was provided by the Air Force Office of Scientific Research. We thank Prof. John Drexler from the Department of Geological Sciences at the University of Colorado for performing the EPMA measurements.We are also grateful to Dr. John Ferguson from the Department of Chemistry and Biochemistry at the University of Colorado for his assistance with the FTIR experiments. We also thank Dr. Alexander Govyadinov for his contribution to the development of anodic alumina membranes.

CM0303080